Dynamic neural network switching for active control of nonlinear systems

Xander Pike; Jordan Cheer (1)



J. Acoust. Soc. Am. 158, 154–163 (2025)

https://doi.org/10.1121/10.0037087





Articles You May Be Interested In

Dynamic neural network switching for active noise control of nonlinear systems

Proc. Mtgs. Acoust. (May 2024)

Feedforward multichannel virtual-sensing active control of noise through an aperture: Analysis on causality and sensor-actuator constraints

J. Acoust. Soc. Am. (January 2020)

Active control of excessive sound emission on a mobile device

J. Acoust. Soc. Am. (April 2015)











Dynamic neural network switching for active control of nonlinear systems

Xander Pike and Jordan Cheera) (D

Institute of Sound and Vibration Research, University of Southampton, Southampton SO17 1BJ, United Kingdom

ABSTRACT:

Feedforward active noise and vibration control systems have been developed for many applications, but are generally designed using linear digital filters, most typically implementing the filtered reference least mean squares algorithm. When the system under control exhibits nonlinearities, linear controllers cannot fully capture the system dynamics to maximize performance. Previous work has shown that neural network (NN) based controllers can improve control performance in the presence of nonlinearities. However, inferring the outputs of NN controllers can be computationally expensive, limiting their practicality, particularly when control is required across a range of nonlinear behaviors. In this paper, a control strategy is proposed where performance is maintained across a nonlinear range of operation by dynamically switching between a set of smaller, and therefore more efficient, NNs that are individually trained over specific ranges of the nonlinear system behavior. It is demonstrated via both simulations of a system with a simple nonlinear stiffness in the primary path and offline simulations using a physical nonlinear dynamical system in the primary path, that the performance of the proposed switching approach offers a control performance advantage compared to both a larger generalized individual NN controller and a functional link artificial neural network based controller.

© 2025 Author(s). All article content, except where otherwise noted, is licensed under a Creative Commons Attribution (CC BY) license (https://creativecommons.org/licenses/by/4.0/). https://doi.org/10.1121/10.0037087

(Received 14 January 2025; revised 3 May 2025; accepted 9 June 2025; published online 7 July 2025)

[Editor: Efren Fernandez-Grande] Pages: 154–163

I. INTRODUCTION

The requirements for the control of unwanted noise and vibration are becoming increasingly stringent in modern engineering systems, with higher levels of control performance required to address user expectations and to manage the increasing requirement for lightweight engineering designs that exacerbate noise and vibration. High frequency noise and vibration can typically be attenuated effectively using passive control solutions. However, the control of low frequency disturbances via passive methods can often require the implementation of large or heavy systems. By comparison, active control solutions are typically capable of achieving effective control at low frequencies, and can benefit from being relatively lightweight and compact.

Historically, feedforward active noise and vibration control systems have been implemented using linear control filters and system models. However, it is well understood that nonlinearities present in either the plant or primary path of the control system can have a significant impact on control performance. ¹⁻⁴ A wide range of approaches have been proposed to overcome this limitation, including polynomial, cross term, or trigonometric expansion of the reference signal, ^{5,6} genetic algorithms, ⁷ and fuzzy logic-based methods. Another methodology that has shown promising results is the application of machine learning methods to these

Many different uses of NNs have been studied in the literature, including system modeling, 4,11–15 feedforward controller design, ^{4,11,16–18} inverse modeling, ¹⁹ signal prediction and feedback control, 20-25 linear filter selection, 26 adaptive parameter estimation for linear controllers, 24,27 frequencydomain control, 28 multichannel controller design, 29 and signal classification.³⁰ However, the ability of such NN control systems to generalize well across a range of system behaviors has not been extensively explored in the associated literature. Nonlinear systems can exhibit rich and varied behavior as the input excitation changes, so training individual NNs to achieve acceptable control performance under such conditions is not straightforward. A training or design approach that provides effective control performance is clearly desirable in practical implementations where the properties of the excitation, and therefore the behavior of the system nonlinearity, may change over time.

It has previously been demonstrated that it is possible to train individual NN controllers to produce control performance over a range of nonlinear system behaviors that approaches the performance of identical NN controllers trained at a single level of nonlinear behavior.³¹ However, the performance of such generalized controllers is dependent on the range of nonlinear behavior over which the



nonlinear control problems. In particular, neural networks (NNs) are well-motivated for both modeling and control of nonlinear systems⁹ due to the fact that they are known to possess the property of being "universal approximators."¹⁰

a)Email: j.cheer@soton.ac.uk

controller is trained to perform well, and the size (and therefore computational cost of inference) of the network. In this paper, a possible solution to this problem is proposed where a set of relatively small NN controllers is trained over distinct operating ranges, and a simple method of switching between these controllers to achieve control performance across a much wider range of operational conditions is proposed.³² Section II describes the simulated nonlinear control problem that is utilised to initially explore the proposed control strategy. Section III describes the proposed controller switching approach, individual controller architecture, and the adopted training methodology. Section IV presents simulation results, which explore how the switched-controller training ranges influence performance and then demonstrate how the performance of the proposed control architecture compares to a larger generalized NN and to an adaptive nonlinear controller. Section V presents a study where the proposed switched-controller approach is applied to a physical nonlinear system, which demonstrates the practicability of the approach for realistic nonlinearities with more complicated characteristics. Finally, Sec. VI discusses conclusions from the work.

II. NONLINEAR CONTROL PROBLEM DEFINITION

A diagram of the simulated nonlinear system to be controlled is presented in Fig. 1. The system consists of a primary source, generating the unwanted disturbance, and a secondary source, which is used to cancel the disturbance. To introduce a nonlinearity into the primary path of the system, the primary source is modeled as a Duffing oscillator. While the type of nonlinearity studied is clearly important, this type of nonlinearity has been utilized in the first instance due to its widespread use within the literature to represent systems with dynamically varying stiffness, as well as its simplicity, with the aim of ensuring that the results of this work are not constrained to an overly-specific problem. Additionally, this system represents a simple use case for the proposed controller-switching approach, since the degree of nonlinear behavior of the system is governed by the magnitude of the system excitation or floor motion, x(t), which is equivalent to the magnitude of the reference signal used by the feedforward control in this case. The secondary source is modeled as a simple harmonic oscillator such that the plant response is linear.

The displacement of the primary source, $y_a(t)$, is induced by displacement of the floor, x(t), to which it is attached. While the motion of the secondary source, y_b , is induced by the control force, u(t), which acts upon it. The equations of motion for the total system can be expressed as

$$m_a \ddot{y}_a(t) + k_a \theta(t) + k_a^{NL} \theta^3(t) + c_a \dot{\theta}(t) = 0,$$
 (1)

$$m_b \ddot{y}_b(t) + k_b y_b(t) + c_b \dot{y}_b(t) + F_c(t) = 0,$$
 (2)

where $\theta(t) = y_a(t) - x(t)$ and the remaining variables are defined in Fig. 1 and Table I. It can be seen from Eq. (1) that the degree of nonlinearity is dependent on the term that

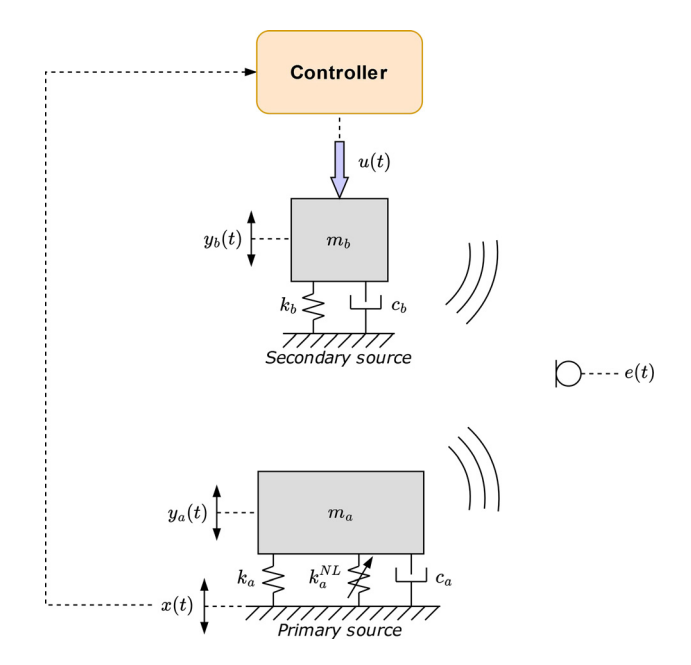


FIG. 1. Diagram of the simulated nonlinear system, consisting of a nonlinear primary acoustic source, and a linear secondary source. System parameters are defined in Table I.

is proportional to the nonlinear stiffness, $k(a)^{NL}$, which depends on both the motion of the floor, x(t), and the motion of the primary mass, $y_a(t)$. However, since the motion of the primary mass is directly dependent on the motion of the floor, the floor motion, which is used as the reference signal in the considered feedforward controller, is an effective measure for the degree of nonlinearity. The parameters that define the dynamics of the simulated system were selected such that the two oscillators have unity mass, but distinct resonance frequencies of 60 and 80 Hz. The damping coefficients c_a and c_b were selected such that each oscillator is subject to 20% of critical damping, such that the oscillators are neither significantly underdamped or overdamped.

The two oscillators are assumed to behave as monopole acoustic sources, with the simplifying assumption that any pressure measurements are made in the far field. The complex far-field pressure field generated by an acoustic monopole oscillating at an angular frequency ω at radius r and time t can be expressed as

$$\tilde{p}(r,\omega,t) = i\frac{Q\rho ck}{4\pi r}e^{i(\omega t - kr)},$$
(3)

TABLE I. Simulated system parameters.

Parameter	Symbol	Value
Primary source mass	m_a	1 kg
Secondary source mass	m_b	1 kg
Primary source linear stiffness	k_a	$1.42 \times 10^5 \text{ Nm}^{-1}$
Primary source cubic stiffness	k_a^{NL}	$1.42 \times 10^{14} \ \text{Nm}^{-3}$
Secondary source stiffness	k_b	$2.53 \times 10^5 \text{ Nm}^{-1}$
Primary source damping	c_a	$151 \; \mathrm{Nsm}^{-1}$
Secondary source damping	c_b	201 Nsm ⁻¹

https://doi.org/10.1121/10.0037087



where Q is the scalar volume velocity of the oscillator, ρ and c are the density and speed of sound of the acoustic medium, respectively, and $k=\omega/c$. For a sphere of radius a oscillating radially with a surface velocity of magnitude U_0 , the volume velocity can be expressed as

$$Q = 4\pi a^2 U_0,\tag{4}$$

and so Eq. (3) can be rewritten as

$$\tilde{p}(r,\omega,t) = i\frac{a^2 U_0 \rho ck}{r} e^{i(\omega t - kr)} = i\frac{a^2 \rho ck}{r} e^{-ikr} \tilde{u}(a,\omega,t),$$
(5)

where $\tilde{u}(a,t) = U_0 e^{i\omega t}$ is the complex velocity of the surface of the oscillating sphere. Under the far-field assumption, the complex pressure and complex source velocity are therefore related by a magnitude scaling factor of $a^2 \rho c k/r$ and a phase change of $\pi/2 - kr$.

In the simulations presented within this paper, x(t) is assumed to be a band-limited Gaussian white noise with a frequency range of [0, 250] Hz. To obtain the pressure produced by each of the two sources, the source velocity, $\dot{y}_a(t)$ or $\dot{y}_b(t)$, is transformed into the frequency domain using a Discrete Fourier transform (DFT), multiplied by $i(a^2\rho ck/r)e^{-ikr}$ as a function of frequency, and inverse Fourier transformed to recover the time-domain pressure. It is assumed that a=1 for both sources, and the distances from the primary and secondary sources to the error sensor are $r_{primary}=2$ m and $r_{secondary}=1$ m, respectively. The system dynamics are simulated in the time-domain using a 4th order Runge-Kutta method at a sample rate of $f_s=2$ kHz.

III. PROPOSED CONTROLLER DESIGN

As noted in Sec. I, it is challenging to train a single NN controller with performance that generalizes across a range of nonlinear behaviors. To overcome this challenge, a dynamic controller switching approach is proposed here where a simple switching process is utilized to select the most suitable controller from a bank of relatively small NN controllers that have been trained to perform over distinct operating ranges, as shown by the proposed controller architecture in Fig. 2. Although this general approach could be used to maintain control performance when the dynamics of the system under control change due various factors, the focus here is on the case where the degree of nonlinear behavior in the system is determined by the magnitude of the signal exciting the primary system, as discussed in Sec. II, which is given by the motion of the floor for the considered system as shown in Fig. 1. From Fig. 2, it can be seen that this signal provides the sampled reference signal, x[n], which is used to both drive the feedforward controller and determine the selection of the most appropriate controller from the controller bank. Specifically, the selection of the controller to be used at a given time instant is determined by comparing an estimate of the root-mean-square (RMS) of the reference signal, x_{RMS} , to the range of reference signal magnitudes over which each controller in the bank of controllers has been trained. x_{RMS} is estimated using a simple moving average process in this paper, the operation of which is determined by two parameters $-t_{update}$ and t_{RMS} . t_{update} is the period between successive calculations of x_{RMS} , and t_{RMS} is the length of the window used for each estimation. This moving average can be expressed as

$$x_{RMS}[n] = \sqrt{\frac{\sum_{i=n-n_{RMS}+1}^{n} x^{2}[i]}{n_{RMS}}},$$
(6)

where n_{RMS} is the number of digital samples in the time period t_{RMS} . The controller trained over the magnitude range containing the current estimate of the reference signal RMS is then utilized to generate the control signal, u[n], for the following time period, t_{update} . Effectively, this results in the weights and biases of the NN being updated dynamically, depending on changes in the magnitude of the reference signal. Although more advanced approaches could be used for the estimation of the RMS, or indeed for selecting the highest performing controller adaptively or using a NN as in Ref. 33 to maximize the control performance, the simple approach has been utilized here to demonstrate that the performance of the proposed strategy is not strongly reliant on a complicated estimation approach.

In order to realize the full dynamically switched-controller described previously, and shown in Fig. 2, it is necessary to design the individual controllers and to specify the ranges over which they are trained. The methodology utilized to train and test the individual controllers is described in Sec. III A, while consideration of the controller training ranges is dependent on the specific system and so is discussed separately in Sec. IV A for the simulated nonlinear system and in Sec. V for the physical nonlinear system.

A. Individual controller architecture and training

The focus of this work is not on the specific network architecture of the individual NN controllers, but on the dynamic switching between controllers. Therefore, all controllers have been implemented as multi-layer perceptron (MLP) networks. Although alternative controller architectures could be utilized, even with the potential to mix different controllers for use over different operational ranges, this is left for future work. Each MLP controller has an input layer of size 160, with further increases having a negligible impact on controller attenuation. Each MLP uses a single hidden layer, with the number of hidden nodes being variously explored, but no significant increase in performance being achieved for the considered system with more than 100 nodes in the hidden layer. A simplified diagram of the individual MLP controller network is provided in Fig. 3, for example.

Similarly to a finite impulse response (FIR) filter, as shown in Fig. 3, the MLP controller takes a tapped delay

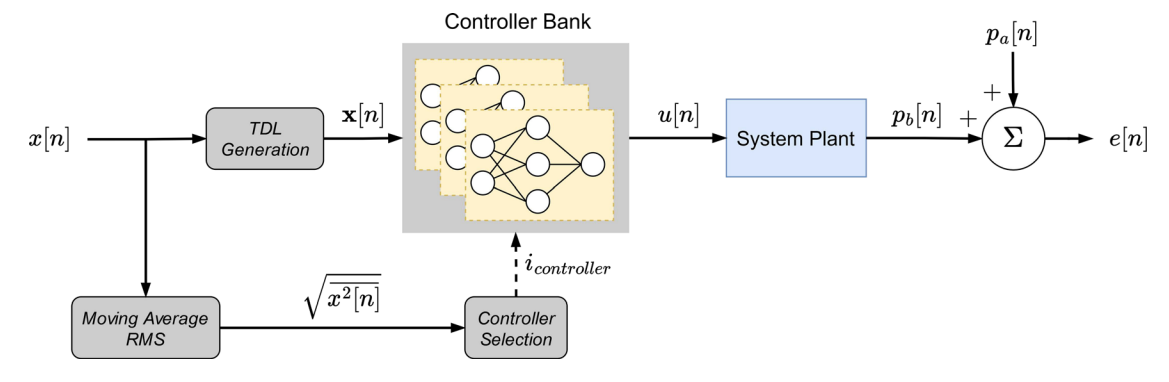


FIG. 2. Block diagram of the controller switching architecture.

line of the digitally sampled reference signal, x[n], as its input, which is given by

$$x[n] = [x[n], x[n-1], ..., x[n-N+1]]^T,$$
 (7)

and the output is the control signal u[n]. However, the MLP differs from an FIR filter in that it also contains a "hidden" layer of values, $\mathbf{h}[n]$, which are calculated from the input tapped delay line as

$$\mathbf{h}[n] = \sigma(\mathbf{W}\mathbf{x}[n] + \mathbf{b}_h),\tag{8}$$

where **W** is a matrix of hidden layer weights, \mathbf{b}_h is a vector of biases associated with the hidden layer, and $\sigma(\bullet)$ is a nonlinear activation function that allows for the network to generate nonlinear mappings and has been defined as a hyperbolic tangent in this case. The network output, u[n], is then given by

$$u[n] = \mathbf{w}_o^{\mathsf{T}} \mathbf{h}[n] + b_o, \tag{9}$$

where \mathbf{w}_o is a vector of output weights, and b_o is an output bias. Combining Eqs. (8) and (9) then gives the network output as

$$u[n] = \mathbf{w}_o^{\mathsf{T}} \sigma(\mathbf{W} \mathbf{x}[n] + \mathbf{b}_h) + b_o.$$
 (10)

1. Controller training

A diagram of the architecture used to train the NN controller is presented in Fig. 4. The training is undertaken

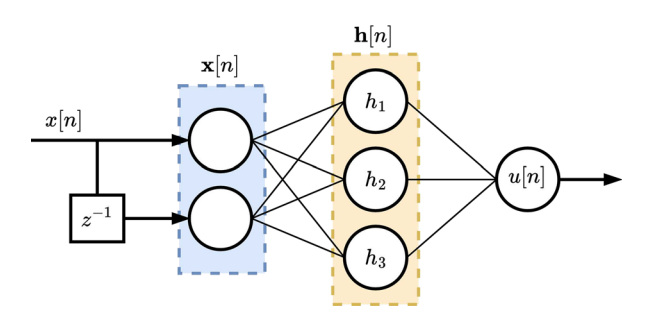


FIG. 3. Block diagram of an example MLP controller network, with an input tapped delay line size of 2, and 3 nodes in the hidden layer.

using the generated reference signal, x[n], and the simulated primary source pressure at the error microphone, $p_a[n]$. To calculate an estimate of the error signal, a Hankel matrix, $\mathbf{X}[n]$ of size $N \times L$ is generated, where N is the tapped delay line length, or input layer size, of the MLP controller, and L is the order of the fixed plant model, $\hat{\mathbf{g}}$, in the discrete time domain. $\mathbf{X}[n]$ can be written as

$$X[n] = \begin{bmatrix} x[n] & x[n-1] & \cdots & x[n-N+1] \\ x[n-1] & x[n-2] & \cdots & x[n-N] \\ \vdots & \vdots & \ddots & \vdots \\ x[n-L+1] & x[n-L] & \cdots & x[n-N-L+2] \end{bmatrix}.$$
(11)

This matrix is passed to the MLP controller, generating a vector $\mathbf{u}[n]$ of length L, which is a tapped delay line of the control signal generated by the current iteration of the controller. The vector $\mathbf{u}[n]$ is subsequently passed to the plant model, generating an estimate, $\hat{p_b}[n]$, of the pressure generated by the secondary source. An estimate of the error signal at the error microphone can then be calculated via the linear summation of the primary and estimated secondary source pressures as $\hat{e}[n] = p_a[n] + \hat{p_b}[n]$. Each controller is trained to minimize the mean squared error (MSE) signal, which is defined as

$$J = \overline{\hat{e}^2[n]},\tag{12}$$

where the mean is calculated over 128 instances of the estimation of the error signal, collectively referred to as a minibatch. The backpropagation algorithm used to update the controller weights and biases was the Adam algorithm with parameters $\alpha=1\times10^{-4}$, $\beta_1=0.9$, $\beta_2=0.99$, and $\epsilon=10^{-7}$. These parameters were selected through trial and error with a view to reaching an effective trade-off between controller performance and training speed. In all cases, the plant model used for controller training was an FIR filter with 160 taps, which was capable of achieving high levels of modeling accuracy due to the linear nature of the simulated plant response.

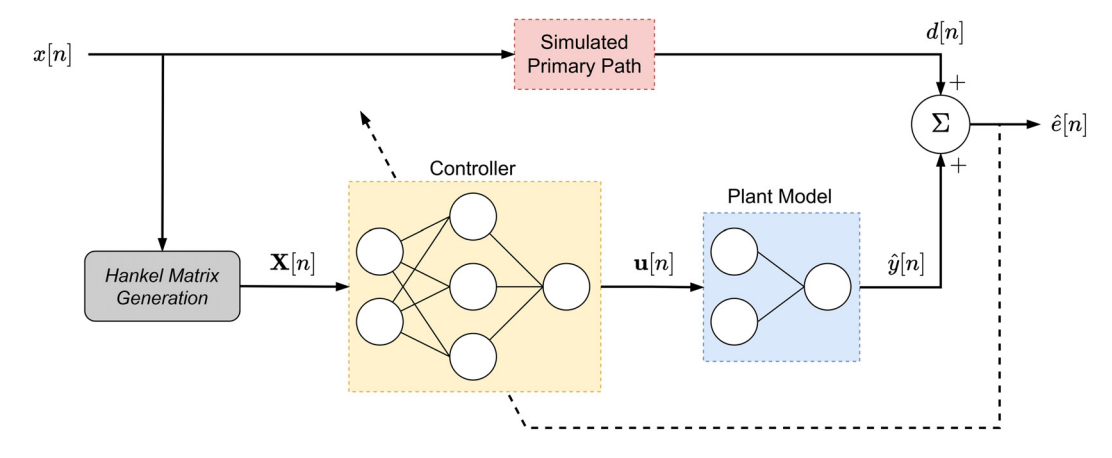


FIG. 4. Block diagram of the controller training method.

To train each network, two sets of 900s of simulated data were generated. The first of the two datasets was used for network training, and the second for validation to assess overfitting. As a result of using this relatively large amount of training data, considering the size of the networks, there was no apparent overfitting during the network training, as assessed via the training and validation losses, and, therefore, network regularization techniques were not applied. Each dataset consists of the reference signal, x[n], which, as noted previously, is a band-limited Gaussian white noise with a frequency range of [0, 250] Hz, and the disturbance signal, $p_a[n]$. In each simulation, the magnitude of the reference signal, or system excitation, increases linearly over time so that it covers the targeted training range in each case. Each update to the weights and biases of the controller networks was undertaken using an average over a minibatch of a tapped delay line of the reference signal and a sample of the disturbance signal. These mini-batches were selected randomly from the generated dataset. In each training step, 1000 such mini-batches were used, and the full network training was undertaken over 500 steps. The term "step" here is used in place of the typical term "epoch" to clarify that the full dataset is not used in each training step, which is explained further in the following.

When training the MLP controllers, it was found that, for a given controller and training range, if the random selection of the training data used to update the network weights and biases had a uniform distribution, then the control attenuation achieved was approximately equal over the training range. However, when training a controller at a single excitation level, it was found that the maximum control attenuation achievable is not uniform over excitation level and, in fact, decreases as the magnitude of the reference signal increases. This means that when using a uniformly distributed selection of training data to train the generalized controllers, their performance approaches the maximum at the upper end of the training range, but falls below the maximum at the bottom. For a set of Q training examples with reference signal magnitudes x_{mag} in the range $a < x_{mag} < b$, the probability of training example q being included in a training batch (up to a normalizing factor) can be defined as

$$P(q) \propto 10^{-\gamma(x_{mag}-a)},\tag{13}$$

where γ is a factor controlling the shape of the probability distribution. Modifying the selection of the training data in this way affects the resultant control attenuation achieved by the MLP controllers across the training range, and an appropriate selection of γ for a given training range results in generalized control performance that approaches the maximum MLP controller performance across the training range. This approach has previously been explored.³¹

IV. SWITCHED-CONTROLLER TUNING AND PERFORMANCE

This section presents simulation results demonstrating the performance of the proposed switch-controller approach. In the first instance, the effect of the controller training range on potential performance is explored, and then the performance of the switched-controller is evaluated. In all cases, simulated data not utilized in the training phase has been utilized.

A. Switched-controller training range analysis

A key parameter in designing the switched-controller system is the selection of the reference signal magnitude ranges over which each controller is trained. This selection should consider both the number of training ranges utilized to cover the overall range of operational conditions and the relative widths of the training ranges. In terms of the relative widths of the training ranges, it has been found that if the overall range is subdivided equally, as shown in the upper image in Fig. 5, this results in under-performance at lower magnitude system excitation levels compared to those trained at higher magnitude levels. This can be related to the fact that the range of behavior exhibited by the nonlinear system is broader for a fixed training width at lower reference signal magnitudes, primarily due to the nature of the assumed nonlinear stiffness. Motivated by this, it has been found that subdividing the overall magnitude range such that the ratio between the widths of neighboring ranges is constant as the reference signal magnitude increases



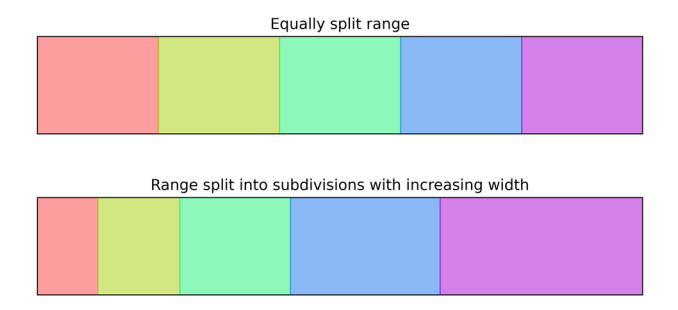


FIG. 5. Examples showing how the full training range of interest may be split into equal subdivisions, or subdivisions with increasing width. In the lower example, the ratio between the widths of neighboring ranges is constant.

provides more consistent performance across the overall range. An example of this proposed subdivision of the full training range is shown in the lower image in Fig. 5.

To explore the effect of varying the number of training ranges, Fig. 6 shows the generalized performance of MLP controllers with between 12 and 100 hidden nodes, trained over subdivisions of three, six, and nine magnitude ranges. In each case, the black dashed lines represent the maximum potential control attenuation achievable, which is determined by using controllers trained and tested at individual reference signal magnitudes, and the colored lines represent the generalized performance of the individual controllers trained over the magnitude ranges denoted by the corresponding colored regions. In both cases, the controllers are tested using 300 s of newly simulated data with a constant excitation magnitude. From the results presented in Fig. 6(a) (three training ranges), it can be seen that with three subdivisions, even increasing the number of hidden nodes substantially from 12 to 100 does not achieve a generalized performance that reaches the estimated maximum performance across the full range. Furthermore, the increase in control performance produced by increasing the number of hidden nodes from 50 to 100 in this case is minimal, suggesting that a further increase in the number of hidden nodes is unlikely to significantly improve performance. From the results presented in Figs. 6(b) (six training ranges) and 6(c) (nine training ranges), for a subdivision of the overall magnitude range into six and nine training ranges, respectively, it can be seen that increasing the number of hidden nodes in the controllers improves their generalized control performance and this approaches the estimated maximum performance as the number of hidden nodes approaches 100. This is perhaps a predictable result, as increasing the number of subdivisions of the full training range approaches the case where the controllers are each trained at a single level. However, comparison of the results presented in Figs. 6(b) and 6(c) illustrates that increasing the number of subdivisions does not necessarily increase the generalized control attenuation for a given number of hidden nodes. Moreover, as there is a computational cost and additional time associated with training each of the individual controllers, it is clear that for any particular application, there will be some optimal number of subdivisions of the full training range

that maximizes generalized control attenuation while minimizing the number of networks required to be trained. Furthermore, although increasing the number of subdivisions may mean that the individual networks require fewer hidden nodes, narrow training regions may result in rapid switching between networks during control, compromising performance.

B. Switched-controller performance analysis

To test the performance of the switched-controller, the set of six controllers with 50 hidden nodes described in Sec. IV A has been utilized since it offers close to maximum performance over the full magnitude range without unnecessarily high training costs. In this instance, the moving average process utilized to dynamically estimate the magnitude of the reference signal as described in Sec. III has been implemented with t_{RMS} and t_{update} set to 0.2 s. To test the performance of the switched-controllers, a dynamically varying excitation condition was simulated over 60 s. Specifically, the magnitude of excitation was first slowly increased from a low to a high value, and then reduced again slowly before rapidly increasing and decreasing. The control attenuation achieved by the switched-controller is presented in Fig. 7, along with the performance achieved by an adaptive normalized-step-size functional link artificial neural network -based (NSS-FLANN) controller35 and a generalized NN trained across the full range of excitation levels. The functional link artificial neural network (FLANN) based controller has been included to provide a benchmark against a commonly utilized adaptive nonlinear control algorithm, while the larger single MLP controller has been included to demonstrate the performance of the switching approach compared to simply utilizing a larger network trained across the full range of operating conditions. From these results, it can be seen that the switched MLP controller is able to achieve effective control attenuation across the range of excitation levels and, as such, closely tracks the maximum steady-state control attenuation for the MLP denoted by the dashed black line. In comparison to the larger generalized MLP controller and the FLANN, the proposed switched MLP controller achieves a consistently higher level of control attenuation. The performance is consistently around 10 dB above the generalized MLP controller, while utilizing half the number of hidden nodes and, therefore, a significantly reduced computational load. A similar performance advantage is also achieved compared to the implemented FLANN, which can also be observed to be relatively slow to regain effective control attenuation following periods of high excitation level.

Despite the effective performance of the switched MLP controller, it is clear from the colored regions in Fig. 7 that there is occasionally quite rapid switching between controllers. It should be noted that this can be addressed by adjusting the t_{update} and t_{rms} parameters used in the RMS estimation procedure. Specifically, with a fixed update rate (t_{update}), a trade-off between accuracy and speed of

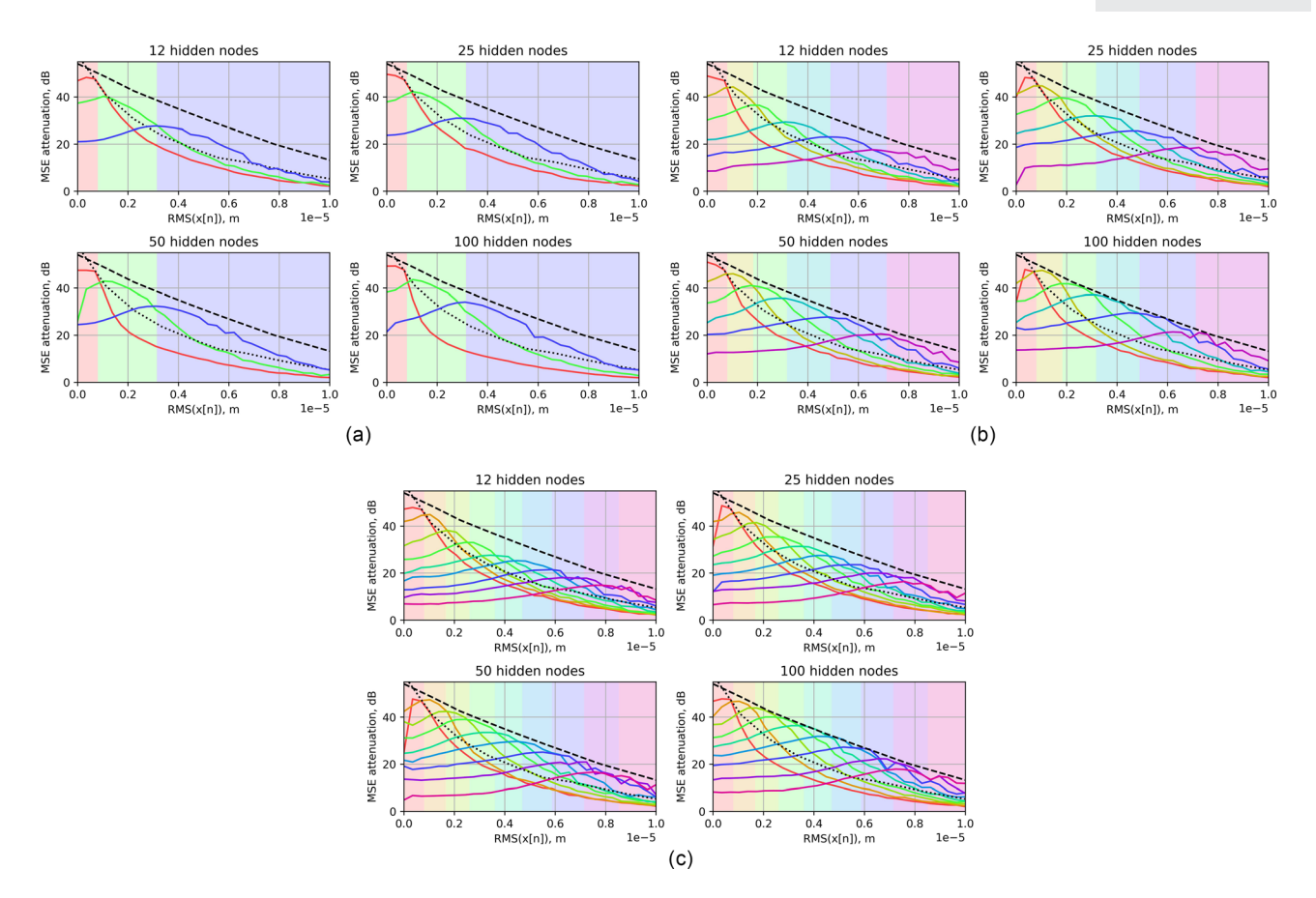


FIG. 6. Generalized performance of controllers trained across three, six and nine training ranges. The black dashed lines indicate the maximum performance achievable by the MLP trained at discrete levels with 100 hidden nodes. The black dotted lines indicate the maximum performance achievable by an FIR controller trained at discrete levels. The colored lines indicate the generalized performance achieved by the individual controllers trained over the excitation signal magnitude ranges defined by the corresponding colored region.

estimation can be realized by adjusting t_{rms} . With a larger t_{rms} the rapid switching can be reduced by obtaining a more accurate estimate of the reference signal RMS, but this will introduce a delay in the estimate and, therefore, the selection of the most appropriate controller. In the case of t_{update} , it is also possible to reduce controller switching by reducing the update rate via an increase in t_{update} , but this would also reduce the ability of the switched-controller to respond to

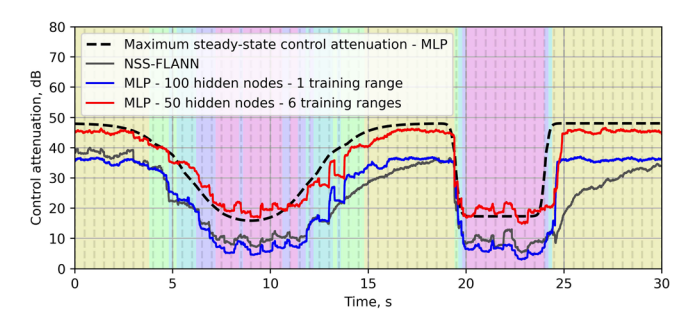


FIG. 7. The control performance achieved when the excitation level, or reference signal magnitude, varies over time for the proposed switched MLP controller, a large MLP trained over the full excitation range, and an NSS-FLANN controller. The MSE control attenuation achieved has been calculated using a 0.5 s moving average. The colored regions represent the selected controller at the corresponding time instance for the switched-controller implementation.

rapid changes in the excitation level. Therefore, both estimation parameters must be tuned for the application, considering the required speed of controller switching to maximize control performance. Alternatively, as noted in Sec. III, it is possible to use a more advanced method of selecting the appropriate controller at any time instant, either via an adaptive approach or in more complicated scenarios via an intelligent approach based on machine learning, as utilized in Ref. 33, to select the most suitable controller for different types of noise. That said, it is clear from the results presented in Fig. 7 that even with the controller switching based on the simple RMS estimation procedure, performance close to the steady-state maximum can be achieved.

V. APPLICATION TO THE CONTROL OF A PHYSICAL NONLINEAR SYSTEM

To further validate the proposed control strategy, its performance when applied to a physical system with a nonlinear response has been explored. The considered experimental system consisted of a thin aluminum plate clamped along its edges by a thick aluminum frame, as shown in Fig. 8. The primary excitation was provided by a small electrodynamic shaker (Tectonic Elements TEAX19C01-8, Tectonic Audio Labs, Woodinville, WA) attached to the surface of the plate, which was overdriven to introduce the



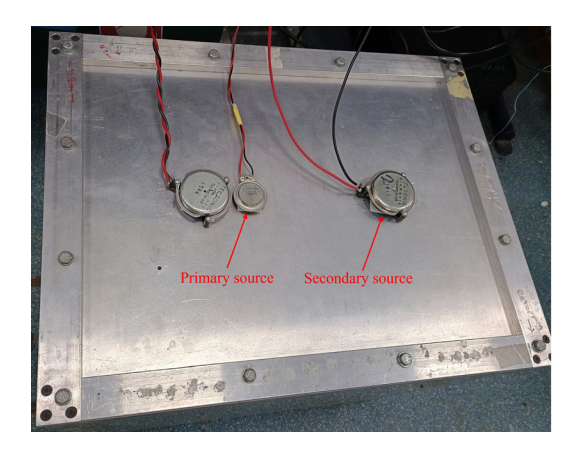


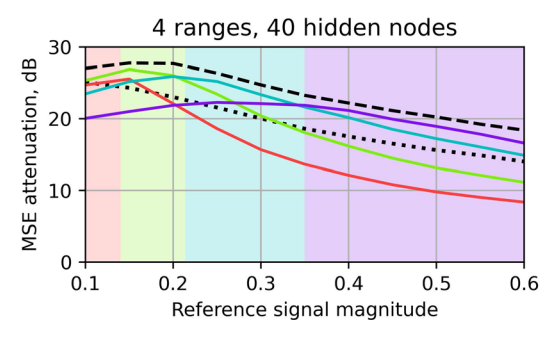
FIG. 8. A photograph of the physical system consisting of a thin aluminum plate with clamped boundaries and electrodynamic shakers providing the nonlinear primary source (left) and secondary source (right). (nb. the third shaker on the left with the same dimensions as the secondary source was not used in this study.)

physical nonlinearity. The secondary source was provided by a larger electrodynamic shaker (Tectonic Elements TEAX32C30-4/B, Tectonic Audio Labs, Woodinville, WA), which was also attached to the surface of the plate. The error sensor was provided by an accelerometer, collocated with the secondary source on the underside of the plate and therefore not visible in Fig. 8. The primary source was driven by low-pass filtered random Gaussian noise, with a cutoff at 250 Hz, and this signal was taken as the reference signal. The system was measured at a sample rate of 2 kHz, and the MLP controllers utilized a hyperbolic tangent activation function and a reference signal tapped delay line length of 0.15 s, corresponding to 300 samples. The estimation of the reference signal RMS was undertaken using the moving average approach described in Sec. III, with $t_{update} = 0.1 \text{ s}$, and $t_{RMS} = 0.5$ s in this case. The data used for the training of the generalized MLP controllers was provided by a measurement of the system excited by a signal that linearly increased in magnitude from a low level to a high level over 150 s, then decreased in magnitude over a further 150 s back to the lower magnitude level. The lower level limit was defined by the noise floor in the system, and the upper limit was chosen to avoid destroying the electrodynamic shaker.

The NN training was undertaken following the same methodology as outlined in Sec. III A 1.

Figure 9 presents the generalized control attenuation calculated via offline simulations for the MLP controllers trained over four ranges with 40 hidden nodes, and nine ranges with 80 hidden nodes, respectively. As was similarly noted in the simulation study presented in Sec. IV A, it can be seen that by increasing the number of training ranges and hidden nodes beyond four ranges and 40 hidden nodes, only a small increase in generalized control performance is achieved. Therefore, the controllers trained over four ranges with 40 hidden nodes were implemented in the following evaluation of the switched MLP controller.

As in Sec. IVB, to test the performance of the switched MLP controller, the excitation signal level was increased from a low level to a high level and back down again, first slowly, then quickly. The upper plot in Fig. 10 presents the results of offline simulations using the measured timehistory of the primary disturbance signal and the measured system responses, and shows the attenuation in the MSE achieved by the switched MLP controller, along with the attenuation achieved by the NSS-FLANN controller and a larger single MLP controller trained over the full range of excitation signal levels. These results show that the switched MLP controller achieves a control performance that is comparable to that of the NSS-FLANN controller during the first 5 s where the excitation level is low and remains relatively constant; however, after both the slow and fast decreases in the excitation signal level (14–19 and 24.5–30 s), the switched MLP controller shows a lower level of control performance. It is possible that this is due to some form of hysteretic behavior induced by the preceding periods of high-level excitation, temporarily changing the dynamics of the system. This is suggested by the fact that during these periods, the control attenuation shows a slow upward trend as the original system response returns. This change in dynamics was not represented in the training data, where the change in excitation signal level was extremely slow, and therefore, it is perhaps unsurprising that the MLP controllers underperform after these changes. To overcome this limitation, rather than retraining the MLP controllers with different excitation signal time-histories, a small augmentation was made to the controller switching approach. Specifically,



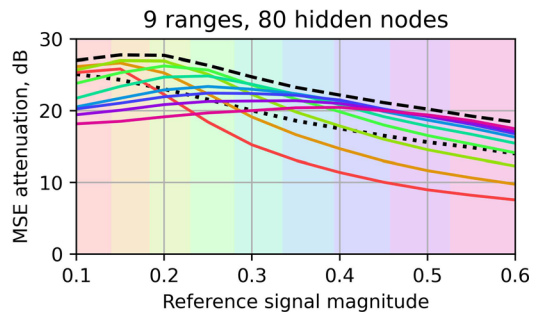


FIG. 9. Generalized performance of controllers trained across 4 ranges with 40 hidden nodes, and 9 ranges with 80 hidden nodes. The black dashed lines indicate the maximum performance achievable by the MLP trained at discrete reference signal magnitudes with 80 hidden nodes. The black dotted lines indicate the maximum performance similarly achievable with an FIR controller.

https://doi.org/10.1121/10.0037087



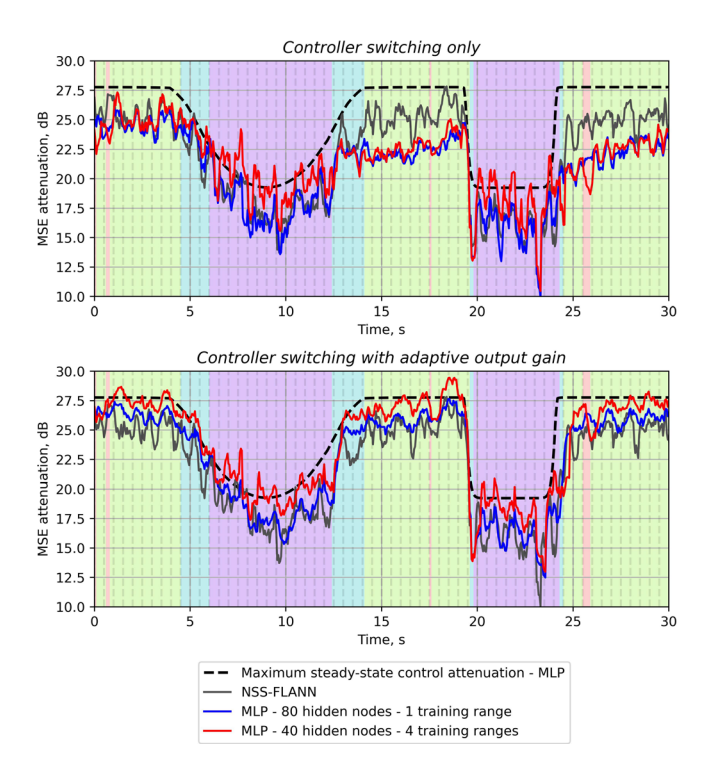


FIG. 10. The control performance achieved for the physical nonlinear system when the excitation level, or reference signal magnitude, varies over time for the proposed switched MLP controller, a large MLP trainined over the full excitation range, and an NSS-FLANN controller. The MSE control attenuation achieved has been calculated using a 0.5 s moving average. The colored regions represent the selected controller at the corresponding time instance for the switched-controller implementation.

an adaptive output gain μ was implemented for each MLP controller, with the gain updated at each sample according to

$$\Delta\mu \propto -e[n]\mathbf{g}^{\mathrm{T}}\mathbf{u}[n],\tag{14}$$

where **g** is an FIR filter modeling the system plant, and $\mathbf{u}[n]$ is a tapped delay line of the previous MLP outputs. It may be noted that, as this update term depends only on the current error signal sample, an FIR plant model, and a TDL of the MLP output, this adaptation will typically come at only a small increase in computational cost. Moreover, the output gain associated with each controller is only updated when that controller is implemented to avoid unnecessary computation. The MSE attenuation levels achieved when the switched MLP controller and the larger single range MLP controller are implemented with an adaptive output gain are presented in the lower plot of Fig. 10. From these results, it can be seen that this simple modification produces a considerable increase in the control performance in both cases. The switched MLP controller with an adaptive output gain now closely follows the MLP maximum attenuation curve, while the larger MLP controller trained over the full range now achieves a comparable performance to the NSS-FLANN.

VI. CONCLUSIONS

In this paper, a method of switching between a set of pre-trained MLP controllers to improve the control

performance achievable for a nonlinear system excited across a range of levels has been presented. Its potential performance has been demonstrated via a set of discrete-time simulations representing the active control of noise produced by a simple nonlinear system, and also via a set of offline simulations using data measured for a more complicated physical nonlinear system. For the presented switched MLP controller, a simple RMS estimator of the magnitude of the reference signal has been used to select from a set of MLP controllers trained to have near-maximal control performance over a set of system excitation magnitude ranges. The effect of increasing the number of training ranges on controller performance has been explored, and the trade-off between computational cost and performance has been discussed. In the numerical simulations of the simple nonlinear system, the switching approach has been shown to achieve control performance that approximates the maximum achievable performance as the reference signal magnitude varies over time. To further validate the proposed control strategy, an offline control simulation has been undertaken using measurements of a physical system with a nonlinear response, which includes both saturation and hysteretic like nonlinear behaviors. In this more realistic case, the proposed switched MLP controller achieved control performance that was significantly lower than the maximum potential attenuation and was outperformed by a well-known adaptive nonlinear control strategy. This was noted to be possibly due to changes in the system dynamics caused by high excitation levels, which were not included in the MLP training data. However, by introducing a simple and computationally efficient adaptive output gain into the MLP controllers, it has been shown that the performance of the switched MLP controller could be significantly increased, outperforming both the well-known adaptive nonlinear controller and a single fixed larger MLP trained across the full range of excitation levels. An earlier version of this work has been published in POMA.³⁶

ACKNOWLEDGMENTS

This work was partially supported by the Intelligent Structures for Low Noise Environments EPSRC Prosperity Partnership (EP/S03661X/1) and by the Department of Science, Innovation and Technology (DSIT) Royal Academy of Engineering under the Research Chairs and Senior Research Fellowships programme. The authors also acknowledge the use of the IRIDIS High Performance Computing Facility and associated support services at the University of Southampton in the completion of this work.

AUTHOR DECLARATIONS Conflict of Interest

J.C. and X.P. have Patent No. WO 2025/012603/A1 pending.

DATA AVAILABILITY

The data that support the findings of this study are available from the corresponding author upon reasonable request.

- ¹X. Pike and J. Cheer, "Limitations of FxLMS in feedforward active vibration control of a nonlinear two-degree-of-freedom system," in *Proceedings of Internoise*, Glasgow, UK (2023), pp. 5219–5229.
- ²M. Costa, J. Bermudez, and N. Bershad, "Stochastic analysis of the filtered-x LMS algorithm in systems with nonlinear secondary paths," IEEE Trans. Signal Process. **50**(6), 1327–1342 (2002).
- ³O. Tobias and R. Seara, "On the LMS algorithm with constant and variable leakage factor in a nonlinear environment," IEEE Trans. Signal Process. **54**(9), 3448–3458 (2006).
- ⁴S. Snyder and N. Tanaka, "Active control of vibration using a neural network," IEEE Trans. Neural Netw. 6(4), 819–828 (1995).
- ⁵L. Tan and J. Jiang, "Adaptive Volterra filters for active control of nonlinear noise processes," IEEE Trans. Signal Process. **49**(8), 1667–1676 (2001).
- ⁶E. Reddy, D. Das, and K. Prabhu, "Fast exact multichannel FSLMS algorithm for active noise control," Signal Process. **89**(5), 952–956 (2009).
- ⁷C. Wangler and C. Hansen, "Genetic algorithm adaptation of non-linear filter structures for active sound and vibration control," in *Proceedings of ICASSP'94*, Adelaide, Australia (1994).
- ⁸Q.-Z. Zhang and W.-S. Gan, "Active noise control using a simplified fuzzy neural network," J. Sound Vib. 272(1-2), 437-449 (2004).
- ⁹S. Chen and S. A. Billings, "Neural networks for nonlinear dynamic system modelling and identification," Int. J. Control 56(2), 319–346 (1992).
- ¹⁰K. Hornik, M. Stinchcombe, and H. White, "Multilayer feedforward networks are universal approximators," Neural Netw. 2(5), 359–366 (1989).
- ¹¹M. Bouchard, B. Paillard, and C. L. Dinh, "Improved training of neural networks for the nonlinear active control of sound and vibration," IEEE Trans. Neural Networks 10(2), 391–401 (1999).
- ¹²K. Narendra and K. Parthasarathy, "Identification and control of dynamical systems using neural networks," IEEE Trans. Neural Networks 1(1), 4–27 (1990).
- ¹³D. Hong, H. Lee, Y. Han, and B. Kim, "Numerical feasibility study for transverse vibration control of rotating shaft with a neural network-based tracking algorithm," in *Proceedings of Internoise 2021*, Washington, DC (2021), pp. 1293–1298.
- ¹⁴H.-S. Kim, "Development of seismic response simulation model for building structures with semi-active control devices using recurrent neural network," Appl. Sci. 10(11), 3915 (2020).
- ¹⁵J. Y. Oh, H. W. Jung, M. H. Lee, K. H. Lee, and Y. J. Kang, "Enhancing active noise control of road noise using deep neural network to update secondary path estimate in real time," Mech. Syst. Sig. Process. 206, 110940 (2024).
- ¹⁶C.-Y. Chang and F.-B. Luoh, "Enhancement of active noise control using neural-based filtered-x algorithm," J. Sound Vib. 305(1), 348–356 (2007).
- ¹⁷D. Chen, L. Cheng, D. Yao, J. Li, and Y. Yan, "A secondary path-decoupled active noise control algorithm based on deep learning," IEEE Signal Process. Lett. 29, 234–238 (2022).
- ¹⁸Y. Guo, D. Shi, X. Shen, J. Ji, and W.-S. Gan, "A survey on adaptive active noise control algorithms overcoming the output saturation effect," Signal Process. 222, 109525 (2024).

- ¹⁹Y. Yan, L. Dong, Y. Han, and W. Li, "A general inverse control model of a magneto-rheological damper based on neural network," J. Vib. Control 28(7), 952–963 (2022).
- ²⁰K. Na and S.-I. Chae, "Single-sensor active noise cancellation using recurrent neural network predictors," in *Proceedings of International Conference on Neural Networks (ICNN'97)*, Houston, TX, pp. 2153– 2156.
- ²¹C. Chen and T.-D. Chiueh, "Multilayer perceptron neural networks for active noise cancellation," in *Proceedings of the 1996 IEEE International Symposium on Circuits and Systems. Circuits and Systems Connecting the World. ISCAS 96*, Atlanta, GA (1996), pp. 523–526.
- ²²M. Salmasi, H. Mahdavi-Nasab, and H. Pourghassem, "Comparison of feed-forward and recurrent neural networks in active cancellation of sound noise," in *Proceedings of the 2011 International Conference on Multimedia and Signal Processing*, Guangxi, China, pp. 25–29.
- ²³T. Matsuura, T. Hiei, H. Itoh, and K. Torikoshi, "Active noise control by using prediction of time series data with a neural network," in *Proceedings of the 1995 IEEE International Conference on Systems, Man and Cybernetics. Intelligent Systems for the 21st Century*, Vancouver, BC, Canada, pp. 2070–2075.
- ²⁴K. Hiramoto and T. Matsuoka, "Active vibration control of structural systems with a preview of a future seismic waveform generated by remote waveform observation data and an artificial intelligence-based waveform estimation system," J. Vib. Control 26(17), 1602–1613 (2020).
- ²⁵Y.-J. Cha, A. Mostafavi, and S. S. Benipal, "Dnoisenet: Deep learning-based feedback active noise control in various noisy environments," Eng. Appl. Artif. Intell. 121, 105971 (2023).
- ²⁶Q. Wang, J. Wang, X. Huang, and L. Zhang, "Semiactive nonsmooth control for building structure with deep learning," Complexity 2017, 6406179 (2017).
- ²⁷J. Liu, X. Li, X. Zhang, and X. Chen, "Modeling and simulation of energy-regenerative active suspension based on BP neural network PID control," Shock Vib. 2019, 1–8.
- ²⁸H. Zhang and D. Wang, "Deep ANC: A deep learning approach to active noise control," Neural Networks 141, 1–10 (2021).
- ²⁹H. Zhang and D. Wang, "Deep MCANC: A deep learning approach to multi-channel active noise control," Neural Netw. 158, 318–327 (2023).
- ³⁰R. Ranjan, J. He, T. Murao, L. Bhan, and W.-S. Gan, "Selective active noise control system for open windows using sound classification," in Proceedings of INTER-NOISE and NOISE-CON Congress and Conference Proceedings (2016), pp. 1921–1931.
- ³¹X. Pike and J. Cheer, "Generalised performance of neural network controllers for feedforward active noise control of nonlinear systems," Acta Acust. 8, 51 (2024).
- ³²An earlier version of this work has been published in the POMA article (Ref. 36).
- ³³Z. Luo, D. Shi, and W.-S. Gan, "A hybrid SFANC-FxNLMS algorithm for active noise control based on deep learning," IEEE Signal Process. Lett. 29, 1102–1106 (2022).
- ³⁴D. Kingma and J. Ba, "Adam: A method for stochastic optimization" (2014).
- ³⁵D. Das and G. Panda, "Active mitigation of nonlinear noise processes using a novel filtered-s LMS algorithm," IEEE Trans. Speech Audio Process. 12(3), 313–322 (2004).
- ³⁶X. Pike and J. Cheer, "Dynamic neural network switching for active noise control of nonlinear systems," Proc. Mtgs. Acoust. 52(1), 055007 (2024).